

# Robotic manipulation of a rotating chain

Hung Pham      Quang-Cuong Pham

**Abstract**—This paper considers the problem of manipulating a uniformly rotating chain: the chain is rotated at a constant angular speed around a fixed axis using a robotic manipulator. Manipulation is quasi-static in the sense that transitions are slow enough for the chain to be always in “rotational equilibrium”. The curve traced by the chain in a rotating plane – its shape function – can be determined by a simple force analysis, yet it possesses a complex multi-solutions behavior typical of non-linear systems. We prove that the configuration space of the uniformly rotating chain is homeomorphic to a two-dimensional surface embedded in  $\mathbb{R}^3$ . Using that representation, we devise a manipulation strategy for transiting between different rotation modes in a stable and controlled manner. We demonstrate the strategy on a physical robotic arm manipulating a rotating chain. Finally, we discuss how the ideas developed here might find fruitful applications in the study of other flexible objects, such as circularly towed aerial systems, elastic rods or concentric tubes.

## I. INTRODUCTION

An idle person with a chain in her hand will likely at some point starts rotating it around a vertical axis, as in Fig. 1A. After a while, she might be able to produce another mode of rotation, whereby the chain would curve inwards, as in Fig. 1B, instead of springing completely outwards. With sufficient dexterity, she might even reach more complex rotation modes, such as in Fig. 1C. Transitions into such complex rotation modes are however difficult to reproduce reliably as instabilities can quickly lead to unsustainable rotations (Fig. 1D). This paper investigates the mechanics of the transitions between different rotation modes, and proposes a strategy to perform those transitions in a stable and controlled manner.

### Motivations

There are several reasons why this problem is hard to solve. First, there are multiple solutions for a given control input (distance  $r$  between the attached end of the chain and the rotation axis, and angular speed  $\omega$ ). This ambiguity makes it difficult to devise a manipulation strategy directly in the control space. Second, some control inputs can quickly lead to “uncontrollable” behaviors of the chain, as illustrated in Fig. 1D.

The theoretical study of the rotating chain and, in particular, of its rotation modes, has a long and rich history in the field of applied mathematics [1], [2], [3], [4], [5], [6], [7], which we review in Section II-A. Here, by devising and implementing

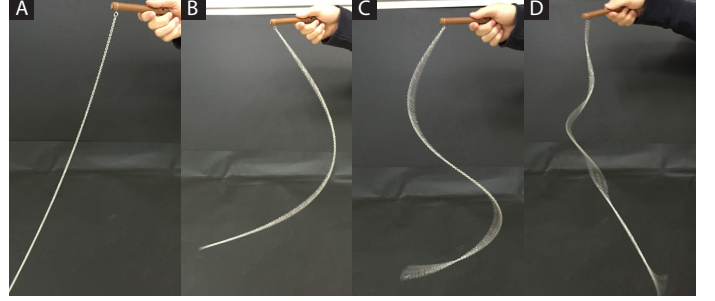


Figure 1. Manual rotation of a chain around a vertical axis. A, B, C: Uniform rotation modes 0, 1, 2 respectively. D: Unstable behavior.

a *manipulation strategy* to stably transit between different rotation modes, we hope to provide a new, robotics-enabled, understanding of this problem. Indeed, at the core of our approach lie concepts specifically forged in the field of robotics, such as “configuration space”, “stable configurations”, “path-connectivity”, etc.

As opposed to rigid bodies, flexible objects are in general characterized by an infinite number of degrees of freedom, which entails significant challenges when it comes to manipulation. Specific approaches have therefore been developed in the field of robotics to study the manipulation of flexible objects, as reviewed in Section II-B.

The above studies are motivated by a number of practical applications. For the rotating chain in particular, applications include aerial manipulation by Unmanned Air Vehicles (UAV), which has recently received some attention, as discussed in more details in Section II-C.

### Contribution and organization of the paper

Our contribution in this paper is threefold. First, we study the case of arbitrary non-zero attachment radii  $r$  (Section IV). This extends and generalizes existing works, which all focus on the case of zero attachment radius, and sets the stage for stable transitions between different rotation modes, which specifically require manipulating the attachment radius. In particular, we determine in this section the number of solutions to the shape equation for any given value  $r$  and  $\omega$ .

Second, we show that the configuration space of the uniformly rotating chain with variable attachment radius is homeomorphic to a two-dimensional surface embedded in  $\mathbb{R}^3$  (Section V). We study the subspace of stable configurations and establish that it is not possible to stably transit between rotation modes without going back to the low-amplitude regime.

Third, based on the above results, we propose a manipulation strategy for transiting between rotation modes in a stable and controlled manner (Section VI). We show the

Hung Pham and Quang-Cuong Pham are with Air Traffic Management Research Institute (ATMRI) and Singapore Centre for 3D Printing (SC3DP), School of Mechanical and Aerospace Engineering, Nanyang Technological University, Singapore. This work was partially supported by grant ATMRI:2014-R6-PHAM (awarded by NTU and the Civil Aviation Authority of Singapore) and by the Medium-Sized Centre funding scheme (awarded by the National Research Foundation, Prime Minister’s Office, Singapore).

strategy in action in a physical experiment where a robotic arm manipulates a rotating chain and makes it reliably transit between different rotation modes.

Before presenting our contribution, we review related works (Section II) and recall Kolodner's equations of motion of the rotating chain (Section III). Finally, we discuss possible applications and extensions and sketch some perspectives for future work (Section VII).

## II. RELATED WORKS

The manipulation of the rotating chain is relevant to a number of fields such as (i) applied mathematics, (ii) flexible object manipulation in robotics, and (iii) aerial manipulation. We now review the literature and describe the position of the current work with respect to each of these fields.

### A. Theoretical studies of the rotating chain

In applied mathematics, the study of the rotating chain was initiated in 1955 by a remarkable paper by Kolodner [1]. Kolodner established the existence of critical speeds  $(\omega_i)_{i \in \mathbb{N}}$  such that there are no uniform rotations if the angular speed  $\omega < \omega_1$ , and there are exactly  $n$  rotation modes for  $\omega_n < \omega < \omega_{n+1}$ . In [2], Caughey studied the rotating chain with small but non-zero attachment radii. The results obtained by Caughey extend Kolodner's and agree with our study of the low-amplitude regime. In [3], Caughey investigated the rotating chain with both ends attached. In [5], Stuart considered the original rotating chain problem using bifurcation theory, and arrived at the same results as Kolodner. In [4], Wu considered the large angular speeds regime. In [7], Toland initiated a new approach based on the calculus of variation, but did not obtain new significant results, as compared to Kolodner.

The common point of all previous works is that the chain is attached to the rotation axis, or very close to it [2]. Yet, reliably observing and transiting between different rotation modes precisely require using arbitrary non-zero attachment radii  $r$ , the distance between the attached end and the rotation axis. The current paper extends previous studies by specifically considering arbitrary attachment radii.

### B. Robotic manipulation of flexible objects

Within the field of robotics, the manipulation of flexible objects is studied along two main directions. A first direction is topological: one is mainly interested in the order and sequence of the manipulation rather than in the precise behavior of the flexible object. Examples include origami folding [8], laundry folding [9] or rope-knotting [10], [11].

The second research direction is concerned with the precise shape and dynamics of the manipulated object. Within this research direction, one can distinguish two main approaches. The first approach discretizes the flexible object into a large number of small rigid elements, and subsequently carries out finite-element calculations, see *e.g.*, [12], [6], [13] for inextensible cables or [14], [15] for concentric tube robots. This approach can be applied to any type of flexible objects as long as a dynamical model is available. However, it usually

yields no *qualitative* understanding of the manipulation. For example, while finite-element calculations can compute the shape of the rotating chain for various control inputs, they can establish neither the existence of different rotation modes, nor the manipulation strategies to transit between different modes.

By contrast, the second approach considers the flexible object as the solution of a (partial) differential equation and tries to establish qualitative properties of this solution. While this approach is harder to put in place – usually because of the complex mathematical calculations and concepts involved – it can lead to stunning and insightful results. For example, Bretl and colleagues established that the configuration space of the Kirchhoff elastic rod is of dimension 6 [16] and that it is path-connected [17]. Such results would be impossible to obtain via finite-element methods.

The present study of the rotating chain is inscribed within this analytical approach. From the dynamic model of the rotating chain, we investigate qualitative properties of its configuration space: dimension, connectivity, and stability. These properties are in turn crucial to devise a manipulation strategy to stably transit between different rotation modes.

### C. Aerial manipulation

Although the study of the rotating chain first stemmed out of scientific curiosity, it has recently found applications in aerial manipulation. In [13], [18], the authors considered a fixed-wing aircraft towing a long cable whose other end is free. The circular flying pattern imprints a pseudo-stationary shape to the cable, which in turn allows precisely controlling the position of the free end. Practical applications of this scheme include remote sensing in isolated areas [18], payload delivery and pickup [12], [19], [18], or more recently, recovery of micro air vehicles [20], [21], [22]. In the latter application, the micro vehicles are able to attach themselves to the towed end, which moves at a relatively slower speed than that of the aircraft. The recent surge of interest in Unmanned Air Vehicles (UAVs) also offers many potential applications: [19] studies a single UAV flying circularly while towing a cable, [23] deals with general (non-circular) aerial manipulation, while [24] targets cooperative manipulation using a team of UAVs.

The above works are based on dynamic simulation [12], [6], [25], or numerical optimal control [22], [26]. Physical experiments were found to agree with simulations [18]. However, there are a number of questions these works are unable to address, for instance: (i) under which conditions are there multiple solutions to the same set of controls (fly radius and angular speed)? (ii) how to avoid or initiate “jumps” between different quasi-static rotational solutions [6]? Here, we precisely answer these questions for the case of a simple rotating chain, without considering aerodynamic drag or end mass. We also discuss how the method can be extended to include these effects, offering thereby solid theoretical foundations for developing safe and stable applications in circular aerial manipulation.

### III. BACKGROUND AND PROBLEM SETTING

#### A. Equations of motion of the rotating chain

Here we recall the main equations governing the motion of the rotating chain initially obtained by Kolodner [1]. Fig. 2 depicts an inextensible and homogeneous chain of length  $L$  and linear density  $\mu$  that rotates around a vertical  $Z$ -axis. One end of the chain is maintained at the attachment radius  $r$  from the rotation axis, while the other end is free. Note that the case of a chain with tip mass can be reduced to this case, see Appendix A.

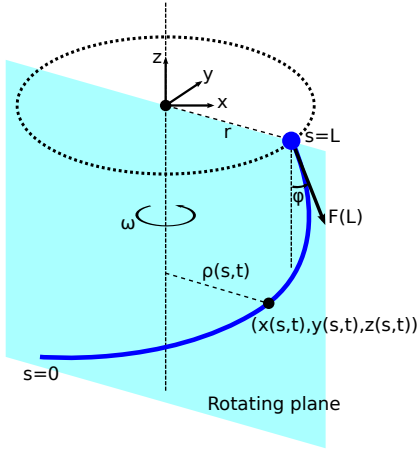


Figure 2. A chain rotating around a fixed vertical axis. At a time instant  $t$ , the chain describes a 3D curve parameterized by  $s$ :  $s = 0$  at the free end,  $s = L$  at the attached end, where  $L$  is the length of the chain.

Let  $\mathbf{x}(s, t) := [x(s, t), y(s, t), z(s, t)]^\top \in \mathbb{R}^3$  denote a length-time parameterization of the chain where  $s$  equals zero at the free end and equals  $L$  at the attached end (Fig. 2). Next, let  $F(s, t) \geq 0$  be the tension of the chain. Neglecting aerodynamic effect, one writes the equation of motion for the chain as

$$\mu \ddot{\mathbf{x}} = (F \mathbf{x}')' + \mu \mathbf{g}, \quad (1)$$

where  $\dot{\phantom{x}}$  and  $\dot{\phantom{x}}'$  denote differentiation with respect to  $t$  and  $s$  respectively;  $\mathbf{g} := [0, 0, -g]^\top$  is the gravitational acceleration vector. The inextensibility constraint can be written as

$$\|\mathbf{x}(s, t)'\|_2 = 1. \quad (2)$$

We seek solutions that are *uniform rotations*; those which have constant shape in a plane that rotates around the  $Z$ -axis. In this case, the motion of the chain becomes

$$\begin{aligned} x(s, t) &= \rho(s) \cos(\omega t), \\ y(s, t) &= \rho(s) \sin(\omega t), \\ z(s, t) &= z(s), \end{aligned} \quad (3)$$

where the function  $\rho(s)$  is called the *shape function* of the chain. Directly from inextensibility constraint (2), we have:

$$\|(\rho(s), z(s))\|_2 = \sqrt{\rho'(s)^2 + z'(s)^2} = 1. \quad (4)$$

Also, the tension of the chain  $F(s, t)$  is time independent.

Substituting the above expressions into Eq. (1) yields

$$(F \rho')' + \mu \rho \omega^2 = 0, \quad (5)$$

$$(F z')' - \mu g = 0, \quad (6)$$

where  $F, \rho, z$  are functions of  $s$ . Integrating Eq. (6) and noting that the tension at the free end vanishes (i.e.,  $F(0) = 0$ ) yield

$$F z' = \int_0^s \mu g \, d\lambda = \mu g s. \quad (7)$$

Next, by the inextensibility constraint (4), we have

$$F = \frac{\mu g s}{z'} = \frac{\mu g s}{\sqrt{1 - \rho'^2}}. \quad (8)$$

Substituting Eq. (8) into Eq. (5) yields the governing equation for the shape function  $\rho(s)$

$$\frac{d}{ds} \left( \frac{\mu g s}{\sqrt{1 - \rho'^2}} \rho' \right) + \mu \rho \omega^2 = 0 \quad (9)$$

subject to the following boundary condition

$$\rho(L) = r. \quad (10)$$

Remark that we have applied two boundary conditions: (i) tension at the free end must be zero:  $F(0, t) = 0$  for any  $t$ ; and (ii)  $\mathbf{x}(L, t)$  equals the reference trajectory traced by the robotic manipulator (or the aircraft's trajectory in the towing problem).

#### B. Problem formulation

We can now define the *configurations* and the *control inputs* of a rotating chain.

**Definition 1.** (*Configuration*) A configuration of the rotating chain is a pair  $q := (\omega, \rho)$ , where  $\omega \geq 0$  is a rotation speed and  $\rho$  is a shape function satisfying the governing equation (9) and that  $\rho(0) \geq 0$ . The set of all such configurations is called the configuration space of the rotating chain and denoted  $\mathcal{C}$ .

**Definition 2.** (*Control input*) A control input is a pair  $(r, \omega)$ , where  $r \geq 0$  is an attachment radius and  $\omega \geq 0$  is a rotation speed. The set of all inputs is called the control space and denoted  $\mathcal{V}$ . If equation (9) has non-trivial solutions with boundary conditions and parameters defined by the input  $(r, \omega)$  then the input is called admissible.

Note that the condition  $\rho(0) \geq 0$  in Definition 1 identifies duplicate solutions. Any configuration  $(\omega, \rho)$  corresponds to two possible solutions: one has shape function  $\rho$  and one has shape function  $-\rho$ , both rotate at angular speed  $\omega$ . The later solution can be obtained by rotating the former solution by 180 degrees. A similar remark applied to the definition of the control space  $\mathcal{V}$  where we require positive attachment radius.

We can formulate the chain manipulation problem as follows: given a pair of starting and goal configurations  $(q_{\text{init}}, q_{\text{goal}})$  find a control trajectory  $(0, 1) \rightarrow \mathcal{V}$  that brings the chain from  $q_{\text{init}}$  to  $q_{\text{goal}}$  without going through instabilities (instabilities will be discussed in Section V-C).

#### IV. FORWARD KINEMATICS OF THE ROTATING CHAIN WITH NON-ZERO ATTACHMENT RADIUS

##### A. Dimensionless shape equation

Still following Kolodner, we convert Eq. (9) into a dimensionless equation, more appropriate for subsequent analyses. Consider the changes of variable

$$u := \frac{\rho'}{\sqrt{1-\rho'^2}} \frac{s\omega^2}{g}, \quad \bar{s} := \frac{s\omega^2}{g}, \quad (11)$$

which by combining with Eq. (9) leads to

$$\frac{du}{d\bar{s}} + \rho \frac{\omega^2}{g} = 0. \quad (12)$$

One can now differentiate Eq. (12) with respect to  $\bar{s}$  to arrive at

$$\frac{d^2}{d\bar{s}^2} u + \rho' = 0,$$

which is combined with the relation

$$\rho' = \frac{u}{\sqrt{\bar{s}^2 + u^2}} \quad (13)$$

to yield the dimensionless differential equation

$$\frac{d^2}{d\bar{s}^2} u(\bar{s}) + \frac{u(\bar{s})}{\sqrt{\bar{s}^2 + u(\bar{s})^2}} = 0. \quad (14)$$

We first consider the boundary condition at  $\bar{s} = 0$ . By definition of  $u$ , one has  $u(0) = 0$ . The end boundary condition  $\rho(L) = r$  implies that

$$u' \left( L \frac{\omega^2}{g} \right) = -r \frac{\omega^2}{g}, \quad (15)$$

where  $\square'$  denotes in this context differentiation with respect to  $\bar{s}$ .

We summarize the boundary conditions on  $u$  as

$$u(0) = 0, \quad u'(\bar{L}) = \bar{r}, \quad (16)$$

where

$$\bar{L} := L\omega^2/g, \quad \bar{r} := -r\omega^2/g. \quad (17)$$

This is the standard form of a Boundary Value Problem (BVP).

**Remark** Denote by  $\rho_0$  the distance from the free end to the Z-axis. Using Eq. (12), we have

$$u'(0) = a, \quad (18)$$

where  $a = -\rho_0\omega^2/g$ .

**Remark** Applying L'Hôpital rule twice, one finds that

$$\lim_{\bar{s} \rightarrow 0} \frac{u(\bar{s})}{\sqrt{\bar{s}^2 + u(\bar{s})^2}} = \frac{a}{\sqrt{1+a^2}}.$$

Thus, the differential equation (14) is well-defined at  $\bar{s} = 0$ .

##### B. Shooting method

We numerically solve the BVP posed in the last section using the *simple shooting method* [27]. Given a control input  $(r, \omega)$ , the method finds resulting configurations as follows:

1. compute  $(\bar{r}, \bar{L})$  from  $(r, \omega)$  using Eq. (17);

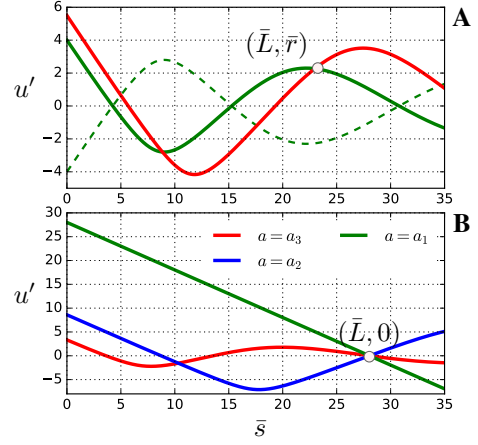


Figure 3. **A:** Shooting from different initial guesses of  $u'(0) = a$ . There might be more than one initial value (green and red) that satisfy the end condition  $u'(\bar{L}) = \bar{r}$ . **B:**  $a_1, a_2, \dots$  are different initial values of  $u'(0)$  that yield  $u'(\bar{L}) = 0$ ;  $a_i$  denotes the initial guess such that the  $i$ -th zero of  $u'$  coincides with  $\bar{L}$ .

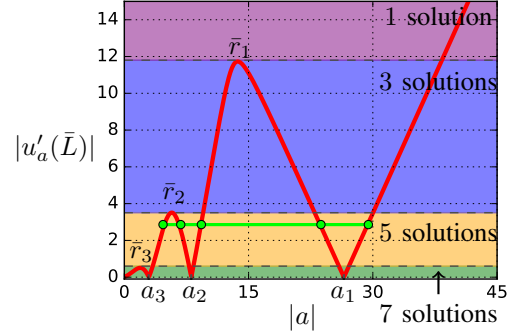


Figure 4. The graph of  $|u'_a(\bar{L})|$  versus  $|a|$ . The main text shows that if  $\bar{r}_{i+1} < |\bar{r}| < \bar{r}_i$ , then there are  $2i + 1$  non-trivial solutions. The green line illustrates the case  $\bar{r}_3 < |\bar{r}| < \bar{r}_2$  where there are 5 non-trivial solutions (green disks).

2. repeat until convergence:

- 2a. guess an initial value  $a \in \mathbb{R}$  for  $u'(0)$  or use the value from the last iteration;
  - 2b. integrate Eq. (14) from the initial condition  $(u(0), u'(0)) = (0, a)$  at  $\bar{s} = 0$  to  $\bar{s} = \bar{L}$ ;
  - 2c. check whether  $u'(\bar{L}) = \bar{r}$ ;
  - 2d. if not, refine the guess  $a$  by e.g., Newton's method;
3. recover  $\rho(s)$  from  $u'_{\text{last\_iter}}(\bar{s})$ .

One can then recover  $z(s)$  using  $\rho(s)$ , the inextensibility constraint (4), the boundary condition  $z(L) = 0$  and the fact that  $z'(s) \geq 0$  (See Eq. (7)). Also, for a given tuple  $(\bar{r}, \bar{L})$ , there might be multiple solutions to the BVP which translates to multiple configurations for a given control input (Fig. 3A).

**Remark** It is straightforward to see that if  $u(\bar{s})_{\bar{s} \in [0, \bar{L}]}$  is a solution of Eq. (14), then  $-u(\bar{s})_{\bar{s} \in [0, \bar{L}]}$  is also a solution. Therefore there is no loss of generality to consider only non-negative values of  $a$ , as integrating from  $-a$  leads to the same configuration.

### C. Number of configuration

We now analyze the number of solutions for different parameters. Denote by  $u'_a(\bar{s})$  the function  $u'(\bar{s})$  obtained by integrating from  $(u(0), u'(0)) = (0, a)$ . Following Kolodner, let  $z_i(a)$  be the  $i$ -th zero of  $u'_a(\bar{s})$ . The function  $z_i(a)$  has the following properties (Theorem 2 [1]):

- $z_i(a)$  is well-defined for all  $i \in \mathbb{N}$  and is a strictly increasing function of  $a$  over  $(0, +\infty)$ ;
- $\lim_{a \rightarrow 0} z_i(a) = h_i^2/4 =: \lambda_i$  where  $h_i$  is the  $i$ -th zero of the Bessel function  $J_0$  (Appendix B);
- $\lim_{a \rightarrow +\infty} z_i(a) = +\infty$ .

Next, let us define  $a_i$  as the absolute value of  $a$  such that  $z_i(a) = \bar{L}$ , i.e.,

$$a_i := |z_i^{-1}(\bar{L})|. \quad (19)$$

By the properties of  $z_i$ ,  $a_i$  exists if and only if  $\lambda_i \leq \bar{L}$  and when it exists, it is unique since  $z_i(a)$  is a strictly increasing function of  $a$ .

Fig. 3B shows the construction of  $a_1, a_2, a_3$ . One can also observe that the  $a_i$ 's form a decreasing sequence, i.e.,

$$a_1 > a_2 > a_3 > \dots > a_n,$$

where  $n$  is the largest  $i$  so that  $\lambda_i \leq \bar{L}$ .

We now turn to the general case where  $\bar{r}$  is not necessarily zero. Consider fixed parameters  $(\bar{r}, \bar{L})$ , it can be seen that the number of configurations equals the number of intersections that the  $u'_a(\bar{L})$  versus  $a$  graph makes with the horizontal lines  $u'_a(\bar{L}) = \bar{r}$  and  $u'_a(\bar{L}) = -\bar{r}$ .

In fact, we can simplify further. Since  $\bar{r}$  and  $-\bar{r}$  refer to the same radius and that  $\rho(s)$  and  $-\rho(s)$  refer to the same shape function, the number of intersections the  $|\bar{\rho}_a(\bar{L})|$  versus  $|a|$  graph makes with the horizontal line  $|u'_a(\bar{L})| = |\bar{r}|$  equals the number of configurations (Fig. 4).

By inspecting Fig. 4,  $|u'_a(\bar{L})|$  is zero at  $a_i$  and  $a_{i+1}$ ; note moreover that  $|u'_a(\bar{L})|$  increases as  $a$  increases from  $a_{i+1}$ , reaches a maximum at some  $a_i^*$ , and then decreases as  $a$  increases from  $a_i^*$  to  $a_i$ <sup>1</sup>. Let us denote the maximum reached by  $|u'_a(\bar{L})|$  between  $a_i$  and  $a_{i+1}$  by  $\bar{r}_i$ , i.e.,

$$\bar{r}_i := |u'_{a_i^*}(\bar{L})| = \max_{a_{i+1} < a < a_i} |u'_a(\bar{L})|, \quad \text{for } i < n; \quad (20)$$

$$\bar{r}_n := \max_{0 < a < a_n} |u'_a(\bar{L})|. \quad (21)$$

One can next observe that the  $\bar{r}_i$ 's form a decreasing sequence<sup>2</sup>, i.e.,

$$\bar{r}_1 > \bar{r}_2 > \bar{r}_3 > \dots > \bar{r}_n.$$

One can now state the following proposition, whose proof results directly from the examination of Fig. 4.

**Proposition 1.** *Let  $n$  be the largest  $i$  so that  $\lambda_i \leq \bar{L}$ . The number of non-trivial configurations of an uniformly rotating chain depends on  $|\bar{r}|$  as follows:*

- 1) if  $|\bar{r}| = 0$ , there are  $n$  non-trivial solutions;
- 2) if  $0 < |\bar{r}| < \bar{r}_n$ , there are  $2n + 1$  non-trivial solutions;

<sup>1</sup>This claim is based on numerical observations.

<sup>2</sup>We have not yet been able to prove rigorously that the sequence is indeed decreasing.

- 3) if  $\bar{r}_{i+1} < |\bar{r}| < \bar{r}_i$  for  $i \in [1, n - 1]$ , there are  $2i + 1$  non-trivial solutions;
- 4) if  $|\bar{r}| = \bar{r}_i$  for  $i \in [1, n]$ , there are  $2i$  non trivial solutions;
- 5) if  $|\bar{r}| > \bar{r}_1$ , there is one non-trivial solution.

### D. Rotation modes

By the change of variable (11),  $u' = \rho\omega^2/g$ , the number of zeros of  $u'(\bar{s})_{\bar{s} \in (0, \bar{L})}$  corresponds to the number of times the chain crosses the rotation axis. We can now give an operational definition of rotation modes.

**Definition 3** (Rotation modes). *A chain is said to be rotating in mode  $i$  if its shape crosses the axis exactly  $i$  times or, in other words, if the function  $u'(\bar{s})_{\bar{s} \in (0, \bar{L})}$  has exactly  $i$  zeros.*

Let us re-interpret Prop. 1 in terms of rotation modes. Consider a positive  $\bar{r}$  verifying  $\bar{r}_{i+1} < \bar{r} < \bar{r}_i$ . In Fig. 4, the horizontal line  $|u'(\bar{L})| = \bar{r}$  intersects the graph of  $|\bar{\rho}_a(\bar{L})|$  versus  $|a|$  at  $2i + 1$  points. Call the  $X$ -coordinates of these points  $b_1 > b_2 > \dots > b_{2i+1}$ . Remark that

- $b_1 > a_1$ , thus by definition of  $a_1$ , the function  $u'_{b_1}(\bar{s})$  has no zero in  $(0, \bar{L})$ , i.e., the chain rotates in mode 0;
- $a_1 > b_2 > b_3 > a_2$ , thus by definition of  $a_1, a_2$ , the functions  $u'_{b_2}(\bar{s})$  and  $u'_{b_3}(\bar{s})$  have each one zero in  $(0, \bar{L})$ , i.e., the chain rotates in mode 1;
- more generally, for any  $k \in [1, i]$ ,  $a_{k-1} > b_{2k} > b_{2k+1} > a_k$ , thus by definition of  $a_{k-1}, a_k$ , the functions  $u'_{b_{2k}}(\bar{s})$  and  $u'_{b_{2k+1}}(\bar{s})$  have each  $k$  zeros in  $(0, \bar{L})$ , i.e., the chain rotates in mode  $k$ .

Figure 5 illustrates the above discussion for  $i = 2$ .

## V. ANALYSIS OF THE CONFIGURATION SPACE OF THE ROTATING CHAIN

In the previous section, we have established a relationship between the control inputs and the configurations. Here, we investigate the properties of the configuration space and of the subspaces of stable configurations. In particular, a crucial question for manipulation, which we address, is whether the stable subspace is *connected*, allowing for stable and controlled transitions between different modes.

### A. Parameterization of the configuration space

From now on, we make two technical assumptions: (i) the distance  $\rho(0)$  from the free end of the chain to the rotation axis is upper-bounded by some  $\rho_{\max}$ ; (ii) the rotation speed  $\omega$  is upper-bounded by some  $\omega_{\max}$ . Note that these two assumptions do not reduce the generality of our formulation since they simply assert that there exist some finite bounds, which could be arbitrarily large. From Eq. (17) and (18), the two assumptions next imply that  $a$  and  $\bar{L}$  are upper-bounded by some constants  $a_{\max}$  and  $\bar{L}_{\max}$ . We can now prove a first characterization of the configuration space.

**Proposition 2** (and definition). *Define the parameter space  $\mathcal{A}$  by*

$$\mathcal{A} := (0, a_{\max}) \times (0, \bar{L}_{\max}).$$

*There exists a homeomorphism  $f : \mathcal{A} \rightarrow \mathcal{C}$ .*



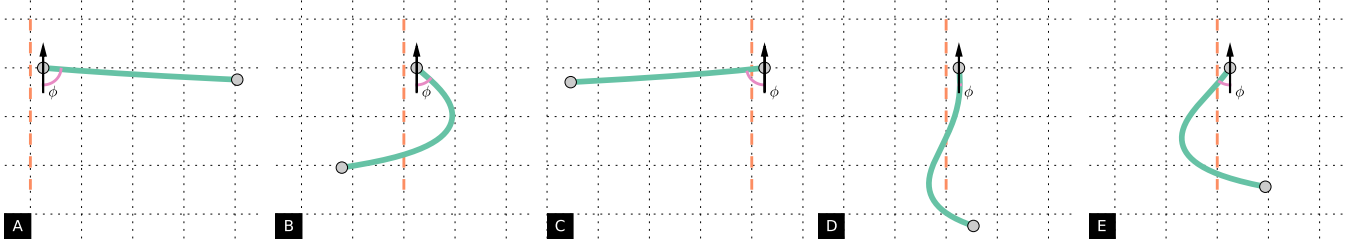


Figure 5. Rotation modes for  $\bar{r}$  where  $\bar{r}_3 < \bar{r} < \bar{r}_2$  ( $i = 2$ ). According to Proposition 1, there are  $2i + 1 = 5$  solutions, depicted in A–E. A rotation is said to be in mode  $i$  if the chain shape crosses the rotation axis (dashed line)  $i$  times. **A**: solution in mode 0, corresponding to  $b_1$  (for the explanation of the numbers  $b_i$ , see main text). **B**, **C**: solutions in mode 1, corresponding to  $b_2, b_3$ . **D**, **E**: solutions in mode 2, corresponding to  $b_4, b_5$ . In addition, the analysis of Section V-C shows that A, B and D are stable, while C and E are unstable.

This proposition implies that, despite (a) the potentially infinite dimension of the space of all shape functions  $\rho$  and (b) the one-to-many mapping between control inputs and configurations, the configuration space of the rotating chain is actually of dimension 2 and has a very simple structure. Note that  $\mathcal{A}$  is essentially a 2D box.

The first dimension,  $a$ , is proportional to the distance of the free end to the rotation axis. Thus, choosing the free end rather than the attached end as reference point allows finding a one-to-one mapping with the shape function. The second dimension,  $\bar{L}$ , is defined by  $\bar{L} := L\omega^2/g$ . Since the length  $L$  of the chain is fixed,  $\bar{L}$  changes as a function of the angular speed  $\omega$ .

To simplify the notations, we define  $\mathbf{u} := (u, u')$  and rewrite Eq. (14) as a dimensionless ODE

$$\frac{d\mathbf{u}}{d\bar{s}} = \mathbf{X}(\mathbf{u}, \bar{s}). \quad (22)$$

We can now give a proof for Proposition 2.

*Proof.* The mapping  $f$  is essentially the shooting method described in Section IV-B. Given a pair  $(a, \bar{L}) \in \mathcal{A}$ , we first obtain  $\omega$  from  $\bar{L}$  using the relationship  $\bar{L} = L\omega^2/g$ . Next, we integrate the ODE (22) from the initial condition

$$\mathbf{u}(0) = (0, a)$$

until  $\bar{s} = \bar{L}$  to obtain  $u'(\bar{s})$  for  $\bar{s} \in (0, \bar{L})$ . Finally, we obtain  $\rho$  from  $u'$  using Eq. (11).

(1) *Surjectivity of  $f$ .* Let  $(\omega, \rho) \in \mathcal{C}$ . Since  $\rho$  verifies (9), one can perform the change of variables (11) and obtain  $u$  and  $u'$ . Next, consider  $a = u'(0)$  and  $\bar{L} = L\omega^2/g$ . One has clearly  $a \in (0, a_{\max})$ ,  $\bar{L} \in (0, \bar{L}_{\max})$ , and  $f((a, \bar{L})) = (\omega, \rho)$ .

(2) *Injectivity of  $f$ .* Assume that there are  $(a_1, \bar{L}_1) \neq (a_2, \bar{L}_2)$  such that  $f(a_1, \bar{L}_1) = f(a_2, \bar{L}_2) = (\omega, \rho)$ . One has  $a_1 = a_2 = -\rho(0)\omega^2/g$  and  $\bar{L}_1 = \bar{L}_2 = L\omega^2/g$ , which implies the injectivity.

(3) *Continuity of  $f$ .* We show in the Appendix C that the ODE (22) is Lipschitz. It follows that the function  $u'(\bar{s})$  for  $0 \leq \bar{s} \leq \bar{L}$  depends continuously on its initial condition, which implies that  $\rho(s)$  depends continuously on  $a$ .

(4) *Continuity of  $f^{-1}$ .* It can be seen from the injectivity proof that  $a$  and  $\bar{L}$  depend continuously on  $\omega$  and  $\rho(0)$ , and the latter depends in turn continuously on  $\rho$ .  $\square$

Next, we establish a homeomorphism between the parameter space and a smooth surface in 3D, which allows an intuitive visualization of the configuration space.

**Proposition 3** (and definition). *For a given  $a \in (0, a_{\max})$ , integrate the differential equation (22) from  $(0, a)$  until  $\bar{s} = \bar{L}_{\max}$ . The set  $(\bar{s}, u(\bar{s}), u'(\bar{s}))_{\bar{s} \in (0, \bar{L}_{\max})}$  is then a 1D curve in  $\mathbb{R}^3$ . The collection of those curves for  $a$  varying in  $(0, a_{\max})$  is a 2D surface in  $\mathbb{R}^3$ , which we denote by  $\mathcal{S}$  (see Fig. 6).*

*There exists a homeomorphism  $l : \mathcal{A} \rightarrow \mathcal{S}$ .*

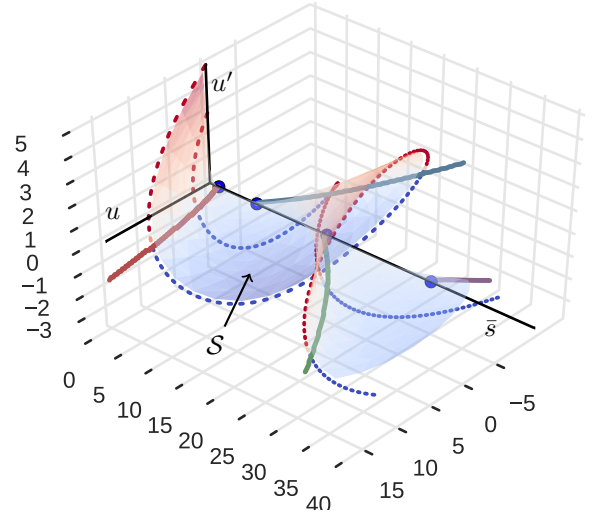


Figure 6. The surface  $\mathcal{S}$  that is homeomorphic to the configuration space  $\mathcal{C}$ . We depict two solution curves on the surface  $\mathcal{S}$  (dashed lines), integrated from two different values of  $a$  (large and medium). Red, blue, green, and purple lines represent respectively the first, second, third and fourth zero-radius loci (see Proposition 4).

*Proof.* The construction of  $l$  follows from the definition: given a pair  $(a, \bar{L}) \in \mathcal{A}$ , integrate (22) from  $(0, a)$  until  $\bar{s} = \bar{L}$ . Then define  $l(a, \bar{L}) := (\bar{L}, \mathbf{u}(\bar{L}))$ .

(1) *Surjectivity of  $l$ .* Consider a point  $(\bar{L}, \mathbf{u}) \in \mathcal{S}$ . By definition of  $\mathcal{S}$ , there exists  $a \in (0, a_{\max})$  so that integrating (22) from  $(0, a)$  reaches  $\mathbf{u}$  at  $\bar{s} = \bar{L}$ . Clearly,  $l(a, \bar{L}) = (\bar{L}, \mathbf{u})$ .

(2) *Injectivity of  $l$ .* This results from the Uniqueness theorem for ODEs, see Appendix C.

(3) Continuity of  $l$ . From the Continuity theorem for ODEs (Appendix C), it is clear that the end point  $(\bar{L}, \mathbf{u}(\bar{L})) \in \mathcal{S}$  depends continuously on the initial condition  $a$ .

(4) Continuity of  $l^{-1}$ . Consider two points  $(\bar{L}_1, \mathbf{u}_1^*), (\bar{L}_2, \mathbf{u}_2^*) \in \mathcal{S}$  that are sufficiently close to each other, i.e.,

$$|\bar{L}_1 - \bar{L}_2| \leq \delta, \quad \|\mathbf{u}_1^* - \mathbf{u}_2^*\| \leq \delta,$$

for some  $\delta$  that we shall choose later. Consider the curves  $\mathbf{u}_1, \mathbf{u}_2$  such that  $\mathbf{u}_1(\bar{L}_1) = \mathbf{u}_1^*$  and  $\mathbf{u}_2(\bar{L}_2) = \mathbf{u}_2^*$ . By the Continuity theorem (Appendix C) one has for some appropriate constant  $K$ ,

$$\begin{aligned} \|\mathbf{u}_1(0) - \mathbf{u}_2(0)\| &\leq e^{M\bar{L}_1} \|\mathbf{u}_1(\bar{L}_1) - \mathbf{u}_2(\bar{L}_1)\| \\ &\leq e^{M\bar{L}_1} (\|\mathbf{u}_1(\bar{L}_1) - \mathbf{u}_2(\bar{L}_2)\| + \|\mathbf{u}_2(\bar{L}_2) - \mathbf{u}_2(\bar{L}_1)\|) \\ &\leq e^{M\bar{L}_1} (\delta + M|\bar{L}_1 - \bar{L}_2|) = e^{M\bar{L}_1} (M + 1)\delta, \end{aligned}$$

where the last inequality come from the uniform boundedness of  $\mathbf{u}$ . For any  $\epsilon$ , it suffices therefore to choose  $\delta := \frac{\epsilon e^{-M\bar{L}_1}}{M+1}$  so that  $\|\mathbf{u}_1(0) - \mathbf{u}_2(0)\| \leq \epsilon$ , which proves the continuity of  $l^{-1}$ .  $\square$

Combining Propositions 2 and 3, we obtain the following theorem.

**Theorem 1.** *The configuration space  $\mathcal{C}$  of the rotating chain is homeomorphic to the 2D surface  $\mathcal{S}$  represented in Fig. 6.*

### B. Zero-radius loci and low-amplitude regime

Before studying the stable subspaces, we need first to define the zero-radius loci and the low-amplitude regime in the configurations space.

**Proposition 4** (and definition). *Zero-radius loci are configurations whose corresponding attachment radii verify  $r = 0$ . Define  $\bar{L}_i := L\omega_i^2/g$  where  $\omega_i$  is the  $i$ -th discrete angular speed (Appendix B). We have the following properties on the surface  $\mathcal{S}$*

- (i) *The  $i$ -th zero-radius locus is an infinite curve that branches out from the  $\bar{s}$ -axis at  $(\bar{L}_i, 0, 0)$ , see Fig. 6;*
- (ii) *The  $i$ -th zero-radius locus separates configurations in rotation mode  $i - 1$  from those in rotation mode  $i$ .*

*Proof.* (i) This property is implied by Kolodner's results, see the first paragraph of Sec IV-C for more details.

(ii) Consider a rotation in mode  $i - 1$  and the corresponding curve  $(\bar{s}, u_1(\bar{s}), u'_1(\bar{s}))_{\bar{s} \in [0, \bar{L}_1]}$ . By definition,  $u'_1(\bar{s})$  has  $i - 1$  zeros in the interval  $[0, \bar{L}_1]$ . Equivalently, we see that the 3D curve  $(\bar{s}, u_1(\bar{s}), u'_1(\bar{s}))$  crosses the first, second, ...,  $i - 1$ -th zero-radius locus. Now, since the loci start infinitely near the  $\bar{s}$ -axis [point (i)] and extend to infinity, any curve deformed from  $(\bar{s}, u_1(\bar{s}), u'_1(\bar{s}))_{\bar{s} \in [0, \bar{L}_1]}$  also crosses the same loci.

Consider now another rotation, which is in mode  $i$ , and the corresponding curve  $(\bar{s}, u_2(\bar{s}), u'_2(\bar{s}))_{\bar{s} \in [0, \bar{L}_2]}$ . By Theorem 1, one can associate the two rotations with their endpoints  $(\bar{L}_1, u_1(\bar{L}_1), u'_1(\bar{L}_1))$  and  $(\bar{L}_2, u_2(\bar{L}_2), u'_2(\bar{L}_2))$  on the surface  $\mathcal{S}$ . We will show that any continuous path that connect these two points necessarily crosses the  $i$ -th zero-radius locus.

Indeed, assume the contradiction, it follows that there is a continuous curve ending at  $(\bar{L}_2, u_2(\bar{L}_2), u'_2(\bar{L}_2))$  that does not cross the  $i$ -th locus. This is a contradiction to our assertion in the first paragraph of point (ii).

We have thus established that the  $i$ -th zero-radius locus separates configurations of rotation mode  $i - 1$  from those in rotation mode  $i$ .  $\square$

**Proposition 5** (and definition). *The low-amplitude regime corresponds to configurations associated with infinitely small values of  $u(\bar{s})$  and  $u'(\bar{s})$ , for all  $\bar{s} \in (0, \bar{L})$ .*

- (i) *The low-amplitude regime corresponds to points on the surface  $\mathcal{S}$  that are infinitely close to the  $\bar{s}$ -axis (in Fig. 6).*
- (ii) *Moreover, this regime corresponds to points on the parameter space  $\mathcal{A}$  that have small values of  $a$ .*

*Proof.* (i) It is clear that a low-amplitude rotation has  $u(\bar{L})$  and  $u'(\bar{L})$  infinitely small. Conversely, if  $u(\bar{L})$  and  $u'(\bar{L})$  are infinitely small, by the continuity of the mapping  $l^{-1}$  in the proof of Proposition 3, the initial condition  $a$  is also infinitely small. Finally, integrating from an infinitely small  $a$  will yield  $u(\bar{s})$  and  $u'(\bar{s})$  infinitely small for all  $\bar{s} \in (0, \bar{L})$ .

(ii) This is true from (i).  $\square$

The low-amplitude rotations with zero attachment radius thus correspond to  $(\bar{L}_i, \delta u, 0)$ ,  $i \in \mathbb{N}$  for small values of  $|\delta u|$ . In the sequel, we shall refer to the  $i$ -th small-amplitude rotation with zero radius as the point  $(\bar{L}_i, 0, 0)$  instead of the more correct phase “ $(\bar{L}_i, \delta u, 0)$  for small values of  $|\delta u|$ ”.

### C. Stability analysis

So far we have considered the space of all configurations of the rotating chain, that is, all solutions to the equation of motion (1). However, not all configurations are *stable*; in fact, experiments show that many are not. This section investigates the structure of the stable subspace – the subset of stable configurations – and discuss stable manipulation strategies.

To analyze the stability of configurations, we model the chain by a series of lumped masses, connected by stiff links, see Fig. 7.

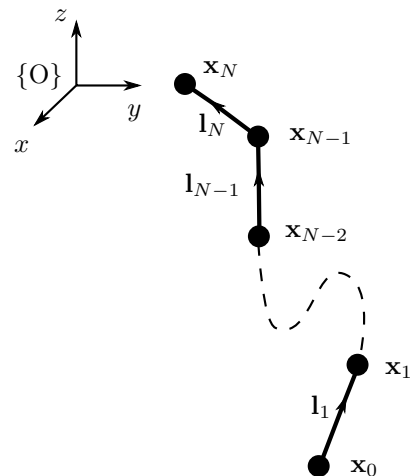


Figure 7. Discretized chain model with  $N$  masses.

Denote the position of the  $i$ -th mass in the rotating frame  $\{O\}$  by  $\mathbf{x}_i \in \mathbb{R}^3$ . The attached end is fixed in  $\{O\}$  at  $\mathbf{x}_N$ . The state of the discretized chain is then given by a  $6N$ -dimensional vector consisting of the positions and velocities of the masses

$$\mathbf{y} := [\mathbf{x}_0, \dot{\mathbf{x}}_0, \dots, \mathbf{x}_{N-1}, \dot{\mathbf{x}}_{N-1}]. \quad (23)$$

Applying Newton's laws to the masses (see details in Appendix D), one can obtain the dynamics equation

$$\dot{\mathbf{y}} = \mathbf{f}(\mathbf{y}). \quad (24)$$

From Proposition 2, the configurations of the rotating chain can be represented by a pair  $(a, \bar{L})$ , which is associated with the position of the free end  $\mathbf{x}_0$ . Next, we discretize  $(0, a_{\max}) \times (0, \bar{L}_{\max})$  into a 2D grid. For each  $(a, \bar{L})$  in the grid, we integrate, from the free end  $\mathbf{x}_0$ , the shape function of the discretized chain (23) at rotational equilibrium – in the same spirit as in Proposition 2. This discretized shape function corresponds to a state vector  $\mathbf{y}^{\text{eq}} := [\mathbf{x}_0^{\text{eq}}, \mathbf{0}, \dots, \mathbf{x}_{N-1}^{\text{eq}}, \mathbf{0}]$ . Finally, we assess the stability of  $\mathbf{y}^{\text{eq}}$  by looking at the Jacobian

$$\mathbf{J}(\mathbf{y}^{\text{eq}}) := \frac{d\mathbf{f}}{d\mathbf{y}}(\mathbf{y}^{\text{eq}}).$$

Specifically, if the largest real part  $\lambda_{\max} := \max_i \text{Re}(\lambda_i)$  of the eigenvalues of  $\mathbf{J}(\mathbf{y}^{\text{eq}})$  is positive, then the system is unstable at  $\mathbf{y}^{\text{eq}}$ ; if it is negative, then the system is asymptotically stable at  $\mathbf{y}^{\text{eq}}$  [28, Theorem 3.1].

Fig. 8(A) depicts the values of  $\lambda_{\max}$  for  $(a, \bar{L}) \in (0, 5) \times (0, 40)$ . One can observe an interesting distribution of these values; in particular, the sharp transitions around the zero-radius loci (black lines). However, even though  $\lambda_{\max}$  gets very close to zero on the left side of the zero-radius loci or in the low-amplitude regime, it is never negative, hinting that the system is at best marginally stable. While this could be expected from our model, which does not include any energy dissipation, it is contrary to the experimental observation of stable rotation states.

We need therefore to take into account aerodynamic forces in the chain dynamics, see details in Appendix D. Note that aerodynamic forces do not significantly affect the analysis of the previous sections, as their effect on the shape of the chain is negligible: for example, for a chain of length 0.76 m and parameters  $(a, \bar{L}) = (2.0, 10.0)$ , the changes in the equilibrium positions are less than 1 mm, which is 0.14% of the chain length.

Fig. 8(B) depicts the values of  $\lambda_{\max}$  for the system with aerodynamic forces. One can note that the overall distribution of  $\lambda_{\max}$  is very similar to that of the system *without* aerodynamic forces [Fig. 8(A)], but with the key difference that the regions in Fig. 8(A) with low but positive values now contain in Fig. 8(B) *negative* values of  $\lambda_{\max}$ , which corresponds to asymptotically stable states.

One can make three more specific observations:

- 1) Configurations that are immediately on the right-hand sides of the zero-radius loci and with  $a$  relatively large are unstable (red color);
- 2) Configurations that are immediately on the left-hand sides

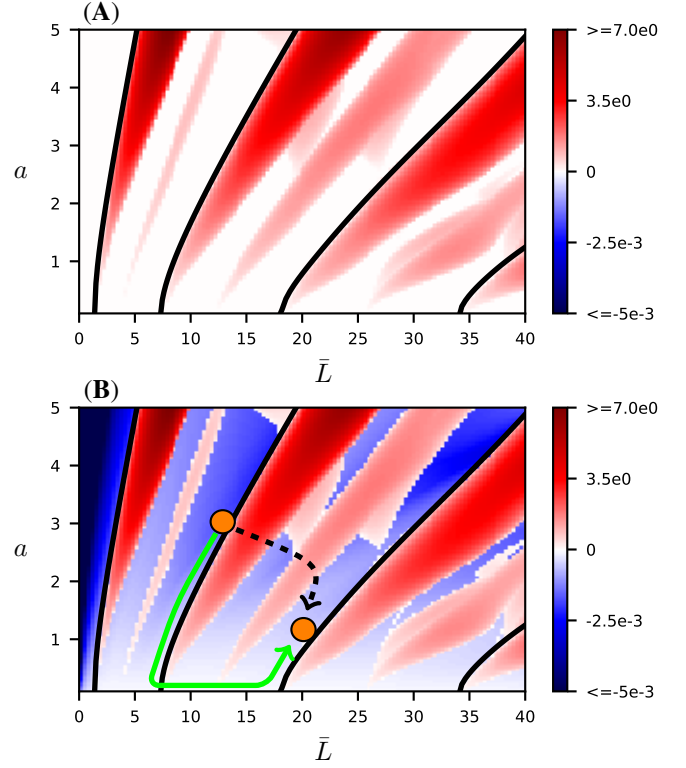


Figure 8. (Best viewed in color) Maps of  $\lambda_{\max}$ , the largest real part of the eigenvalues of the linearized dynamics of two 10-link lumped-mass models at equilibrium: (A) model without aerodynamic forces and (B) model with aerodynamic forces. Positive values (red color) indicate unstable behaviors while negative values (blue color) indicate asymptotically stable behaviors. Most configurations that are stable in the presence of aerodynamic forces can not be concluded to be stable when there is no aerodynamic forces. Black lines: zero-radius loci – configurations whose attachment radii are zeros. Green arrow: A path in the chain's configuration space that contains only stable configurations. Black dashed arrow: A path that contains unstable configurations.

of the zero-radius loci and with  $a$  relatively large are stable (blue color);

- 3) Configurations with  $a$  small (low-amplitude regime) are stable (light blue color).

Observation (1) hints that the upper portions of the zero-radius loci form “unstable barriers” in the configuration space. Therefore, it is *not* possible to stably transit between rotation modes  $i - 1$  and  $i$  (which requires crossing the  $i$ -th zero-radius locus, see Proposition 4) while staying in the upper portion of the configuration space [dashed black arrow in Fig. 8(B)]. Observation (2) implies that transitions between configurations of the same mode can be stable. Observation (3) hints that a possible transition strategy might consist in (i) going down to the low-amplitude regime; (ii) traversing the  $i$ -th zero-radius locus while remaining in the low-amplitude regime; (iii) going up towards the desired end configuration [green arrow in Fig. 8(B)]. This strategy thus traverses only regions with negative  $\lambda_{\max}$  and can be expected to be stable. The next section experimentally assesses this strategy.



## VI. MANIPULATION OF THE ROTATING CHAIN

### A. Experiment

We now experimentally test the manipulation strategy enunciated in the previous section. More precisely, to stably transit between two different rotation modes  $i$  and  $j$ , we propose to [see the green arrow in Fig. 8(B)]

- 1) Move from the rotation of mode  $i$  towards  $(\bar{L}_{i+1}, 0, 0)$  while staying in the blue region of Fig. 8(B);
- 2) Move along the  $\bar{L}$ -axis towards  $(\bar{L}_{j+1}, 0, 0)$ ;
- 3) Move from  $(\bar{L}_{j+1}, 0, 0)$  towards the rotation of mode  $j$  while staying in the blue region of blue region of Fig. 8(B).

In practice, the histories of the control inputs ( $r$  and  $\omega$ ) to achieve the transitions in steps 1 and 3 can be found by simple linear interpolation, see e.g. Fig. 9(A).

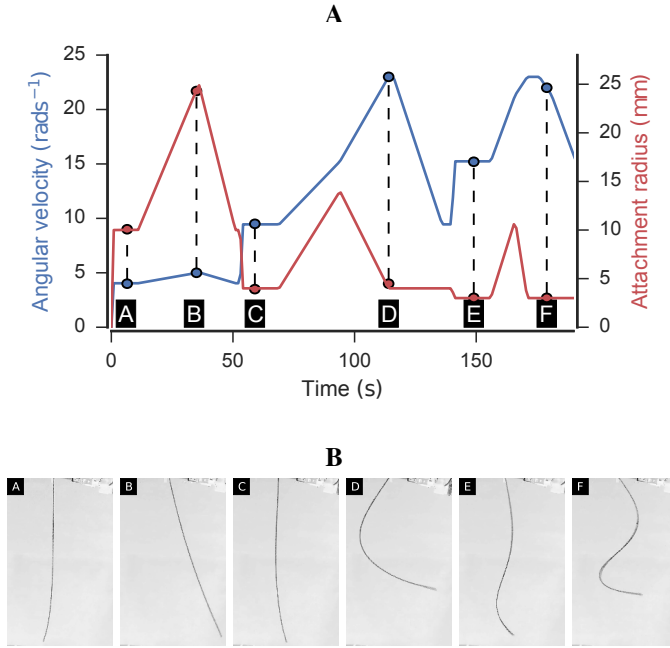


Figure 9. **A**: Histories of the control inputs. Red: attachment radius  $r$ ; blue: angular speed  $\omega$ . **A**: low-amplitude rotation at critical speed  $\omega_1$ . **A**  $\rightarrow$  **B**: moving deep into rotation mode 0. **B**: stable rotation at mode 0. **B**  $\rightarrow$  **C**: moving back to the low-amplitude regime with critical speed  $\omega_1$  and subsequently increasing the speed to  $\omega_2$  while staying in the low-amplitude regime. **C**: low-amplitude rotation at critical speed  $\omega_2$ . **C**  $\rightarrow$  **D**: moving deep into rotation mode 1. **D**: stable rotation at mode 1. **E**: low-amplitude rotation at critical speed  $\omega_3$ . **F**: stable rotation at mode 2. Note that the attachment radius was not exactly zero in the low-amplitude regimes, but set to some small values. This was necessary to physically generate the desired rotation speeds. **B**: Snapshots of the chain at different time instants. The labels A–F refer to the same time instants as in the control inputs plot. A video of the experiment (including more types of transitions) is available at <https://youtu.be/EnJdn3XdxEE>.

We perform the following transitions

Rest  $\rightarrow$  Mode 0  $\rightarrow$  Mode 1  $\rightarrow$  Mode 2

on a metallic chain of length 0.76 m (note that the weight of the chain is not involved in the calculations). The upper end of the chain was attached to the end-effector of a 6-DOF industrial manipulator (Denso VS-060). The critical speeds, calculated using equation (36), are given in Table I.

Table I  
CRITICAL SPEEDS FOR A CHAIN OF LENGTH 0.76 m

$i$	1	2	3
$\omega_i$ (rad s $^{-1}$ )	4.34	9.97	15.64

A video of the experiment (including more types of transitions) is available at <https://youtu.be/EnJdn3XdxEE>. Fig. 9(A) shows the attachment radius and the angular speed as functions of time. Fig. 9(B) shows snapshots of the chain at different rotation modes. As can be observed in the video, the chain could transit between different rotation modes in a stable and controlled manner.

As the final note, we observed that any manipulation sequence that traverses highly unstable regions (red regions in Fig. 8) definitely leads to unsustainable rotations, as illustrated by the last section of the video.

### B. Implications for aerial manipulation

For a circularly towing system, the ability to transit between rotation modes is desirable. Indeed, different modes have different functions. For instance, mode 0 rotations are most suitable to initiate a rotation sequence from a straight flying trajectory. On the other hand, rotations at higher order modes such as 1 and 2 have more compact shapes, smaller tip radii and higher tip velocities, and are therefore more suitable to perform the actual deliveries or explorations.

It is furthermore desirable to switch modes in a quasi-static manner, as studied in this paper. Indeed, the *transient* dynamics of a heavily underactuated system such as the chain can be difficult to handle. The infinite dimensionality of the system, unavoidable modeling errors and aerodynamic effects make it challenging to design and reliably execute non-quasi-static mode switching trajectories.

Our result suggests however that it is *not* possible to realize quasi-static mode transitions with fixed-wing aircraft. Indeed, since the turning radii of such aircraft are lower-bounded, the resulting rotations cannot enter the low-amplitude regime, which is necessary for quasi-static mode transition, as shown in the above development. Therefore, although non-quasi-static mode transitions are more challenging to plan and execute, they must be studied in future works.

## VII. CONCLUSION

The study of the rotating chain has a long and rich history. Starting from the 1950's, a number of researchers have described its behavior, and identified the existence of rotation modes. In this paper, we have investigated for the first time the *manipulation* problem, *i.e.*, how to stably transit between different rotation modes. For that, we developed a framework for understanding the kinematics of the rotating chain with non-zero attachment radii and its configuration space. Based on this understanding, we proposed a manipulation strategy for transiting between different rotation modes in a stable and controlled manner. In turn, on the practical side, this result has some implications for aerial manipulation.

It can be shown (see Appendix A) that all the previous developments can be extended to the case of the chain with non-negligible tip mass. The key enabling notion here is that of *differential flatness* [13], with the flat output being the state of the free end. By differential flatness, given any trajectory of the free end, one can reversely compute the state trajectory and the control trajectory of the whole system. In fact, the property that we have “manually” discovered in this paper – the configuration space of a rotating chain is parameterized by the parameter space  $\mathcal{A}$  – is related to the differential flatness of the rotating chain system. Indeed, each point  $(a, \bar{L})$  corresponds to a circular motion of the free end, which in turn, by differential flatness, corresponds to the state and control trajectory of the whole chain, which in turn defines the configuration. This observation suggests two possible extensions:

- the motion of the free end can be more general (*e.g.*, an ellipse), and can thereby lead to more practical applications, such as swinging to hit some position with the tip mass;
- other differentially-flat systems, whose flat output can be parameterized.

Another idea developed here, namely the visualization of the configuration space based on forward integration of the shape function, might find fruitful applications in the study of other flexible objects with “mode transition”, such as elastic rods or concentric tubes subject to “snapping”. Our future work will explore these possible extensions.

## APPENDIX

### A. Chain with non-negligible tip mass

Suppose that the free end of the chain carries a drogue of mass  $M$ . We show that all the previous development can be applied to this more general problem.

We first proceed similarly to Section III and derive the dynamics equation of the rotating chain with tip mass. Writing the force equilibrium equation at the tip mass yields

$$F(0)z'(0) = Mg, \quad (25)$$

$$F(0)\rho'(0) = -M\rho(0)\omega^2. \quad (26)$$

Next, integrate Eq. (25) to obtain

$$F(s)z(s)' = g(\mu s + M), \quad (27)$$

where  $\mu$  is again the linear density of the chain. This equation leads to

$$F(s) = g \frac{\mu s + M}{\sqrt{1 - \rho'^2}}. \quad (28)$$

One arrives at the governing equation

$$\frac{d}{ds} \left( \rho' \frac{\mu s + M}{\sqrt{1 - \rho'^2}} \right) + \rho \frac{\mu \omega^2}{g} = 0, \quad (29)$$

with boundary condition  $\rho(L) = r$  where  $r$  is the attachment radius. One can now convert Eq. (29) to a dimensionless equation

$$\frac{d^2 u}{d\bar{s}^2} + \frac{u}{\sqrt{(\bar{s} + M\omega^2/\mu g)^2 + u^2}} = 0 \quad (30)$$

by the following changes of variable

$$\begin{aligned} u &:= \rho' \frac{\mu s + M}{\sqrt{1 - \rho'^2}} \frac{\omega^2}{\mu g}, \\ \bar{s} &:= \frac{s\omega^2}{g}. \end{aligned} \quad (31)$$

The boundary conditions are

$$u'(0) = a, \quad (32)$$

$$u(0) = a \frac{M\omega^2}{\mu g}, \quad (33)$$

$$u'(\bar{L}) = \bar{r}, \quad (34)$$

where  $a = -\rho(0)\omega^2/g$  and  $\bar{r} = -r\omega^2/g$ .

Eq. (30) is a BVP that can be solved using the shooting method as described in Section IV-B. Moreover, we see that  $(a, \bar{L})$  also parameterizes the solution space, which is the configuration space of the rotating chain with tip mass.

### B. Low-amplitude regime

Here we recall the results obtained by Kolodner [1] for the low-amplitude regime. Low-amplitude rotations are defined by a zero attachment radius  $r = 0$  and infinitely small values for the shape function  $\rho$ . Linearizing equation (9) about  $\rho = 0$  yields

$$\rho\omega^2/g + \rho' + s\rho'' = 0, \quad (35)$$

with the boundary condition  $\rho(L) = 0$ .

By a change of variable  $v := 2\sqrt{s\omega^2/g}$ , one can rewrite the above equation as

$$\rho v + \rho_v + \rho_{vv}v = 0,$$

which has solutions of the form

$$\rho(v) = cJ_0(v), \quad \text{i.e.,}$$

$$\rho(s) = cJ_0(2\omega\sqrt{s/g}),$$

where  $J_0$  is the zeroth-Bessel function. The boundary condition  $\rho(L) = 0$  then implies that the angular speed can only take discrete values  $(\omega_i)_{i \in \mathbb{N}}$  where

$$\omega_i = \frac{h_i}{2} \sqrt{g/L} \quad (36)$$

where  $h_i$  is the  $i$ -th zero of the Bessel function  $J_0$ .

### C. Useful results from the theory of Ordinary Differential Equations

**Lemma 1** (Lipschitz). *The ordinary differential equation (22) satisfies Lipschitz condition in some convex bounded domain  $\mathcal{D}$  that contains  $\mathcal{S}$ .*

*Proof.* Note first that  $|u''(u, \bar{s})| < 1$  for all  $u, \bar{s} \in \mathbb{R}$ , which implies that  $\mathcal{S}$  is bounded. Set now

$$\mathcal{D} := (0, \bar{L}_{\max}) \times (u_{\inf}, u_{\sup}) \times (u'_{\inf}, u'_{\sup}),$$

where  $u_{\inf}$ ,  $u_{\sup}$ ,  $u'_{\inf}$ ,  $u'_{\sup}$  are bounds on  $\mathcal{S}$ . Clearly,  $\mathcal{D}$  is bounded, convex and contains  $\mathcal{S}$ . Next, all partial derivatives

$\frac{\partial \mathbf{X}_i}{\partial x_j}$  are continuous in  $\mathcal{D}$  (with continuation at  $\bar{s} = 0$ , see Remark in Section IV-A). This implies that  $\mathbf{X}$  is Lipschitz in  $\mathcal{D}$  [29].  $\square$

We now recall two standard theorems in the theory of Ordinary Differential Equations, see *e.g.*, [29].

**Theorem 2** (Uniqueness). *If the vector field  $\mathbf{X}(\mathbf{u}, t)$  satisfies Lipschitz condition in a domain  $\mathcal{D}$ , then there is at most one solution  $\mathbf{u}(t)$  of the differential equation*

$$\frac{d\mathbf{u}}{dt} = \mathbf{X}(\mathbf{u}, t)$$

*that satisfies a given initial condition  $\mathbf{u}(a) = \mathbf{c} \in \mathcal{D}$ .*

**Theorem 3** (Continuity). *Let  $\mathbf{u}_1(t)$  and  $\mathbf{u}_2(t)$  be any two solutions of the differential equation  $\mathbf{X}(\mathbf{u}, t)$  in  $T_1 \leq t \leq T_2$ , where  $\mathbf{X}(\mathbf{u}, t)$  is continuous and Lipschitz in some domain  $\mathcal{D}$  that contains the region where  $\mathbf{u}_1(t)$  and  $\mathbf{u}_2(t)$  are defined. Then, there exists a constant  $M$  such that*

$$\|\mathbf{u}_1(t) - \mathbf{u}_2(t)\| \leq e^{M|t-a|} \|\mathbf{u}(a) - \mathbf{y}(a)\|$$

*for all  $a, t \in [T_1, T_2]$ .*

#### D. The discretized chain model

Here we describe the procedure to obtain Eq. (24), which is the dynamics equation of the discretized chain model employed in Section V-C, see also Fig. 7.

The net force  $\mathbf{F}_i$  acting on the  $i$ -th mass is the sum of the following three components:

- 1) *fictitious forces*, which include the Coriolis force and centrifugal force associated with the rotating frame;
- 2) *constraint forces* generated by the  $i$ -th and  $i+1$ -th links;
- 3) *aerodynamic forces*, which include drag and lift.

Fictitious forces are computed using standard formulas, which can be found in any textbook on classical mechanics. To compute the constraint forces, we model the links as stiff linear springs whose stiffness approximates that of the chain used in the experiment of Section VI, which was  $\simeq 8 \times 10^7$  N/m. Constraint forces are then computed using Hooke's law.

Next, to compute aerodynamic forces, we follow the modelling choices of [18], *i.e.* the aerodynamic forces acting on the  $i$ -th link is placed entirely on the  $i$ -th mass. Specifically, define the link length vector as  $\mathbf{l}_i := \mathbf{x}_i - \mathbf{x}_{i-1}$  and denote by  $\mathbf{v}_i$  the actual air speed of the  $i$ -th mass, the angle of attack of the  $i$ -th link is given by

$$\cos \xi_i = -\frac{\mathbf{l}_i \cdot \mathbf{v}_i}{\|\mathbf{l}_i\| \|\mathbf{v}_i\|}.$$

The drag and lift acting on the  $i$ -th link are then given by

$$\begin{aligned} \mathbf{F}_i^D &= 0.5 \rho_a C_D \|\mathbf{l}_i\| d \|\mathbf{v}_i\|^2 \mathbf{e}_D, \\ \mathbf{F}_i^L &= 0.5 \rho_a C_L \|\mathbf{l}_i\| d \|\mathbf{v}_i\|^2 \mathbf{e}_L, \end{aligned}$$

where the directions and coefficients of drag and lift are

$$\begin{aligned} \mathbf{e}_D &= -\frac{\mathbf{v}_i}{\|\mathbf{v}_i\|}, & \mathbf{e}_L &= -\frac{(\mathbf{v}_i \times \mathbf{l}_i) \times \mathbf{v}_i}{\|(\mathbf{v}_i \times \mathbf{l}_i) \times \mathbf{v}_i\|}, \\ C_D &= C_f + C_n \sin^3(\xi_i), & C_L &= C_n \sin^2 \xi_i \cos \xi_i. \end{aligned}$$

In the above equations,  $d$  denotes the diameter of the chain,  $C_f$  and  $C_n$  are respectively the skin-friction and crossflow drag coefficients,  $\rho_a$  is the air density. These parameters have the following numerical values

$$\begin{aligned} d &= 1 \text{ mm}, & \rho_a &= 1.225 \text{ kg/m}^3, \\ C_f &= 0.038, & C_n &= 1.17. \end{aligned}$$

Summing the components we obtain the  $i$ -th net force  $\mathbf{F}_i$ , from which the acceleration of the  $i$ -th mass can be found as

$$\ddot{\mathbf{x}}_i = \mathbf{F}_i / m_i,$$

where  $m_i$  is the mass of the  $i$ -th mass. Rearranging the terms, one obtains the dynamics equation (24)

$$\dot{\mathbf{y}} = \mathbf{f}(\mathbf{y}).$$

#### REFERENCES

- [1] I. I. Kolodner, "Heavy rotating string – a nonlinear eigenvalue problem," *Communications on Pure and Applied Mathematics*, vol. 8, no. 3, pp. 395–408, aug 1955.
- [2] T. K. Caughey, "Whirling of a heavy chain," in *Third U. S. National Congress of Applied Mechanics*, 1958.
- [3] —, "Large Amplitude Whirling of an Elastic String—a Nonlinear Eigenvalue Problem," *SIAM Journal on Applied Mathematics*, vol. 18, no. 1, pp. 210–237, jan 1970.
- [4] C.-H. Wu, "Whirling of a String at Large Angular Speeds—A Nonlinear Eigenvalue Problem with Moving Boundary Layers," *SIAM Journal on Applied Mathematics*, vol. 22, no. 1, pp. 1–13, jan 1972.
- [5] C. A. Stuart, "Steadily rotating chains," in *Applications of Methods of Functional Analysis to Problems in Mechanics*. Springer, 1976, pp. 490–499.
- [6] J. J. Russell and W. J. Anderson, "Equilibrium and Stability of a Circularly Towed Cable Subject to Aerodynamic Drag," *Journal of Aircraft*, vol. 14, no. 7, pp. 680–686, 1977.
- [7] J. Toland, "On the stability of rotating heavy chains," *Journal of Differential Equations*, vol. 32, no. 1, pp. 15–31, apr 1979.
- [8] D. J. Balkcom and M. T. Mason, "Robotic origami folding," *The International Journal of Robotics Research*, vol. 27, no. 5, pp. 613–627, 2008.
- [9] S. Miller, J. Van Den Berg, M. Fritz, T. Darrell, K. Goldberg, and P. Abbeel, "A geometric approach to robotic laundry folding," *The International Journal of Robotics Research*, vol. 31, no. 2, pp. 249–267, 2012.
- [10] H. Wakamatsu, E. Arai, and S. Hirai, "Knotting/un knotting manipulation of deformable linear objects," *The International Journal of Robotics Research*, vol. 25, no. 4, pp. 371–395, 2006.
- [11] Y. Yamakawa, A. Namiki, and M. Ishikawa, "Dynamic High-speed Knotting of a Rope by a Manipulator," *International Journal of Advanced Robotic Systems*, p. 1, 2013.
- [12] R. a. Skop and Y. I. Choo, "The configuration of a cable towed in a circular path," *Journal of Aircraft*, vol. 8, no. 11, pp. 856–862, 1971.
- [13] R. M. Murray, "Trajectory generation for a towed cable system using differential flatness," in *IFAC world congress*, 1996, pp. 395–400.
- [14] H. B. Gilbert, D. C. Rucker, and R. J. W. Iii, "Concentric Tube Robots: The State of the Art and Future Directions," *International Symposium on Robotics Research*, pp. 1–16, 2013.
- [15] D. C. Rucker, B. A. Jones, and R. J. Webster, "A model for concentric tube continuum robots under applied wrenches," in *Proceedings - IEEE International Conference on Robotics and Automation*, 2010, pp. 1047–1052.
- [16] T. Bretl and Z. McCarthy, "Quasi-static manipulation of a kirchhoff elastic rod based on a geometric analysis of equilibrium configurations," *The International Journal of Robotics Research*, vol. 33, no. 1, pp. 48–68, 2014.
- [17] A. Borum and T. Bretl, "The free configuration space of a kirchhoff elastic rod is path-connected," in *Robotics and Automation (ICRA), 2015 IEEE International Conference on*. IEEE, 2015, pp. 2958–2964.

- [18] P. Williams and P. Trivailo, "Dynamics of Circularly Towed Aerial Cable Systems, Part I: Optimal Configurations and Their Stability," *Journal of Guidance, Control, and Dynamics*, vol. 30, no. 3, pp. 753–765, 2007.
- [19] M. Merz and T. A. Johansen, "Feasibility study of a circularly towed cable-body system for UAV applications," in *Unmanned Aircraft Systems (ICUAS), 2016 International Conference on*. IEEE, 2016, pp. 1182–1191.
- [20] M. B. Colton, L. Sun, D. C. Carlson, and R. W. Beard, "Multi-vehicle dynamics and control for aerial recovery of micro air vehicles," *International Journal of Vehicle Autonomous Systems*, vol. 9, p. 78, 2011.
- [21] J. Nichols and L. Sun, "Autonomous Aerial Rendezvous Of Small Unmanned Aircraft Systems Using A Towed Cable System," *Journal of Guidance, Control, and Dynamics*, vol. 37, no. 4, pp. 1–12, 2014. [Online]. Available: <http://arc.aiaa.org/doi/abs/10.2514/1.62220>
- [22] L. Sun, J. D. Hedengren, and R. W. Beard, "Optimal Trajectory Generation using Model Predictive Control for Aerially Towed Cable Systems," *{AIAA} Journal of Guidance, Control and Dynamics*, vol. 37, no. 2, pp. 525–539, 2014.
- [23] K. Sreenath, N. Michael, and V. Kumar, "Trajectory generation and control of a quadrotor with a cable-suspended load-a differentially-flat hybrid system," in *Robotics and Automation (ICRA), 2013 IEEE International Conference on*. IEEE, 2013, pp. 4888–4895.
- [24] N. Michael, J. Fink, and V. Kumar, "Cooperative manipulation and transportation with aerial robots," *Autonomous Robots*, vol. 30, no. 1, pp. 73–86, 2011.
- [25] P. Williams, D. Sgarioto, and P. M. Trivailo, "Constrained path-planning for an aerial-towed cable system," *Aerospace Science and Technology*, vol. 12, no. 5, pp. 347–354, 2008.
- [26] P. Williams and P. Trivailo, "Dynamics of Circularly Towed Cable Systems, Part 2: Transitional Flight and Deployment Control," *AIAA Journal of Guidance, Control, and Dynamics*, vol. 30, no. 3, pp. 766–779, 2007.
- [27] J. Stoer and R. Bulirsch, "Introduction to Numerical Analysis," p. 96, 1982.
- [28] H. K. Khalil, *Nonlinear Systems*. Prentice-Hall, New Jersey, 1996.
- [29] J. Hu and W.-P. Li. (2005) Theory of ordinary differential equations. [Online]. Available: <https://www.math.ust.hk/~mamu/courses/303/Notes.pdf>